

This paper is a postprint of a paper submitted to and accepted for publication in IET Radar, Sonar & Navigation and is subject to Institution of Engineering and Technology Copyright. The copy of record is available at IET Digital Library.

Experimental Demonstration and Analysis of Cognitive Spectrum Sensing and Notching for Radar

Brandon Ravenscroft^{1*}, Jonathan W. Owen¹, John Jakabosky¹, Shannon D. Blunt¹, Anthony F. Martone², Kelly D. Sherbondy²

¹Radar Systems Lab (RSL), University of Kansas, Lawrence, KS, USA

²Sensors and Electron Devices Division, Army Research Laboratory (ARL), Adelphi, MD, USA

*G171r597@ku.edu

Abstract: Spectrum sensing and transmit notching is a form of cognitive radar that seeks to reduce mutual interference with other spectrum users in the same band. This concept is examined for the case where another spectrum user moves in frequency during the radar's CPI. The physical radar emission is based on a recent FM noise waveform possessing attributes that are inherently robust to sidelobes that otherwise arise for spectral notching. Due to increasing spectrum sharing with cellular communications, the interference considered takes the form of in-band OFDM signals that hop around the band. The interference is measured each PRI and a fast spectrum sensing algorithm determines where notches are required, thus facilitating a rapid response to dynamic interference. To demonstrate the practical feasibility and to understand the trade-space such a scheme entails, free-space experimental measurements based on notched radar waveforms are collected and synthetically combined with separately measured hopping interference under a variety of conditions to assess the efficacy of such an approach, including the impact of interference hopping during the radar CPI, latency in the spectrum sensing/waveform design process, notch tapering to reduce sidelobes, notch width modulation due to spectrum sensing, and the impact of digital up-sampling on notch depth.

1. Introduction

Generally speaking, cognitive radar (also referred to as fully adaptive radar) seeks to make the sensing function more proactive in terms of the selection/design of the waveform(s) and/or other transmit parameters (e.g. centre frequency, pulse repetition frequency etc.) based on a variety of possible observations about the environment such as target/clutter characteristics and spectral occupancy by other radio frequency (RF) users [1–7]. The particular focus here is on the automated generation of physically realisable waveforms that possess spectral notches to avoid in-band interference. Such a condition is expected to become ever more problematic with the continued proliferation of 4G and eventually 5G communication systems into radar bands [8–10].

The notion of spectrally notching radar waveforms as a means of RF interference (RFI) avoidance has been considered by many [11–23], with a recent survey from an optimisation theory perspective appearing in [24]. While the majority of such approaches involve spectral notching of a single waveform or by extension the same waveform over the coherent processing interval (CPI), it was shown in [16] that doing so incurs a rather significant penalty in terms of increased radar range sidelobes. However, it was recently experimentally demonstrated [22, 23, 25, 26] that the spectral notching of frequency modulated (FM) noise waveforms [27, 28] largely avoids this limitation because the incoherent combining of range sidelobes across multiple distinct pulsed waveforms in the CPI serves to reduce the resulting sidelobe

level by a factor commensurate with the number of pulses [29].

Here the FM noise waveform spectral notching capability is incorporated into a cognitive radar framework that performs spectrum sensing on a per-pulse basis, estimates the spectral footprint of any in-band interference, and then adjusts the notch location(s) and width(s) in an automated manner. The fast spectrum sensing (FSS) algorithm [30, 31], which mimics the rapid data assimilation capability of the human thalamus [32], is used to quickly estimate the frequency intervals requiring notching. For interference taking the form of frequency-hopping orthogonal frequency division multiplexed (OFDM) communications, this overall cognitive strategy employs FSS to inform the subsequent notching of FM noise waveforms, with the ultimate goal of achieving real-time RFI avoidance.

Using experimental loopback measurements of OFDM interference and separate free-space radar measurements obtained with the resulting notched waveforms, the impact to the radar is evaluated through the synthetic combination of these data sets. It is demonstrated that, given a hypothetical ability to sense changes in the interference spectral location(s) instantaneously, a significant signal-to-interference-plus-noise ratio (SINR) enhancement is obtained for the moving target indication (MTI) application. However, this enhancement is shown to be limited by the latency in the sense/design process. That said it is also demonstrated that a simple blanking procedure [33] for the affected pulse(s) can be used to compensate somewhat for this degradation. Additional practical effects that are assessed include tapering

of the notch edges to reduce range sidelobes, modulation of the notch width due to temporal variations in the spectral sensing stage, and the limiting effects of digital up-sampling on notch depth and how it can be compensated.

The following section surveys a recent scheme to design spectrally notched FM waveforms that are physically realisable given knowledge of the notch locations/widths. Section 3 summarises a recent low-latency approach to estimate the spectral content of in-band RFI so as to facilitate rapid modifications to notched FM noise waveforms in dynamic environments. Section 4 then examines the implementation of these waveforms in actual hardware, with particular attention paid to up-sampling/up-conversion for deployment on an arbitrary waveform generator (AWG) and practical amplification effects with regard to notch depth. In Section 5, the efficacy of these notched waveforms is examined from a point-spread function perspective, with the specific effects of notch tapering, Doppler spread of clutter, and notch width modulation due to spectrum sensing variability being considered. The interference rejection capability of spectral notches is then evaluated in Section 6. Finally, Section 7 presents some case studies using free-space MTI measurements that demonstrate both the practical prospects and open research problems to make cognitive spectral notching a reality.

2. FM Noise Waveforms

This cognitive radar framework takes advantage of a recently developed FM noise radar waveform denoted as pseudo-random optimised (PRO) FM [27, 28]. As a brief review, PRO-FM waveforms are unique and change on a pulse-to-pulse basis, with each individual waveform possessing relatively low-range sidelobes due to spectral shaping such that the corresponding power spectrum approximates a Gaussian shape [34]. However, their true utility arises from (1) being FM, so that they are readily amenable to high-power transmission, and (2) when combined in Doppler processing after pulse compression, where it is observed that the unique sidelobe structures combine incoherently to further suppress the sidelobes. Due to the spectral shaping construction, this type of waveform has also been shown to readily permit the inclusion of spectral notches [22].

Consider the design of a pulsed FM waveform with duration T and 3 dB bandwidth B , which is simultaneously required to possess favourable (i.e. low) autocorrelation sidelobes. The FM nature inherently imposes a constant amplitude envelope and relatively good spectral containment (compared to phase codes); attributes that provide robustness to the distortion incurred by a high-power transmitter. The m th pulsed waveform is initialised with a random instantiation of a polyphase-coded FM (PCFM) waveform [35], denoted as $s_{0,m}(t)$. To facilitate optimisation, the corresponding (length N) discretised version $\mathbf{s}_{0,m}$ is employed, which is sufficiently ‘over-sampled’ with respect to 3 dB bandwidth to provide adequate fidelity for the discretised waveform (i.e. minimal aliasing) via inclusion of a good portion of the spectral roll-off region.

This discretised waveform undergoes K iterations of the alternating projections

$$\mathbf{r}_{k+1,m} = \mathbb{F}^{-1} \left\{ \mathbf{g} \odot \exp \left(j \angle \mathbb{F} \{ \mathbf{s}_{k,m} \} \right) \right\} \quad (1)$$

and

$$\mathbf{s}_{k+1,m} = \mathbf{u} \odot \exp \left(j \angle \mathbf{r}_{k+1,m} \right). \quad (2)$$

Here \mathbb{F} and \mathbb{F}^{-1} are the Fourier and inverse Fourier transforms, respectively, $\angle(\bullet)$ extracts the phase of the argument, and \odot is the Hadamard product. The length N vector \mathbf{g} is a discretisation of the desired spectrum $|G(f)|$, while the length N vector \mathbf{u} is a discretisation of rectangular window $u(t)$ that has duration T .

The projection in (1) serves to match the power spectrum of the FM waveform to a power spectrum template denoted as $|G(f)|^2$. We choose this template to be a Gaussian shape so that the associated autocorrelation likewise has a Gaussian shape [34], though the shape is arbitrary. The signal $\mathbf{r}_{k+1,m}$ resulting from the first stage has a power spectrum matching the desired $|G(f)|^2$, but does not possess a constant amplitude. Thus, the projection in (2) enforces constant amplitude by removing the amplitude modulation (AM). This alternating process is repeated for K iterations. In the experimental analysis that follows, K was arbitrarily set to 100, though more sophisticated stopping criteria could be used as well.

The presence of a narrowband interference source(s) can be addressed by incorporating spectral notch(es) into the template via the null constraint

$$|G(f)| = 0 \text{ for } f \in \Omega, \quad (3)$$

where Ω represents the frequency interval(s) of the desired notch(es). The inclusion of rectangular notches in the spectrum has been shown [22] to induce a $\sin(x)/x$ roll-off in the autocorrelation sidelobes, thus degrading the autocorrelation response. However, inclusion of a taper in the spectral region surrounding the notch(es) through

$$|G(f)| = \begin{cases} h_L(f) & \text{for } f \in \Omega_L \\ 0 & \text{for } f \in \Omega \\ h_U(f) & \text{for } f \in \Omega_U \end{cases} \quad (4)$$

has been demonstrated to be an effective solution [23]. Here the frequency intervals Ω_L and Ω_U indicate the lower and upper frequency regions around the notch, to which are applied the tapers $h_L(f)$ and $h_U(f)$, respectively. A gradual transition between a notch and its local power spectrum is attained by forcing each tapered region to be continuous with its surrounding power spectrum. The shape of the taper regions can be arbitrary, but it has been observed that use of a Tukey taper compensates for the $\sin(x)/x$ sidelobe roll-off rather well [23].

Enforcing the null constraint in (3) can produce spectral notches with depths on the order of roughly 20 dB relative to the local power spectrum level. If deeper spectral notches are desired, the reiterative uniform weight optimisation (RUWO) technique [20] has been shown to attain appreciably deeper notches when applied after the optimisation process above. Since this process is also iterative, the final vector $\mathbf{s}_{K,m}$ from (2), which well approximates the continuous signal $s_{K,m}(t)$ due to the preservation of good spectral containment in (1) by the proper choice of $|G(f)|^2$ and sufficient ‘over-sampling’, is now denoted as $\mathbf{x}_{0,m}$.

In the RUWO formulation each frequency interval Ω to null in (3) is discretised into Q frequency values f_q , such that the $N \times Q$ matrix \mathbf{B} comprised of discretised frequency steering vectors can be formed as

$$\mathbf{B} = \begin{bmatrix} 1 & 1 & \dots & 1 \\ e^{j2\pi f_0} & e^{j2\pi f_1} & \dots & e^{j2\pi f_{Q-1}} \\ \vdots & \vdots & \ddots & \vdots \\ e^{j2\pi f_0(N-1)} & e^{j2\pi f_1(N-1)} & \dots & e^{j2\pi f_{Q-1}(N-1)} \end{bmatrix}. \quad (5)$$

An $N \times N$ structured matrix is subsequently obtained by

$$\mathbf{W} = \mathbf{B}\mathbf{B}^H + \delta\mathbf{I}, \quad (6)$$

where \mathbf{I} is an $N \times N$ identity matrix and δ is a diagonal loading term. Performing L iterations of RUWO via

$$\mathbf{x}_{l,m} = \exp\left(j\angle\left(\mathbf{W}^{-1}\mathbf{x}_{l-1,m}\right)\right) \quad (7)$$

for each pulse (indexed by m) serves to deepen the spectral notch obtained via the PRO-FM process. Since sufficient over-sampling with respect to the 3 dB bandwidth is maintained throughout, the vector $\mathbf{x}_{L,m}$ approximates, with high fidelity, the continuous-time signal $x_{L,m}(t)$.

3. Spectrum Sensing & Notch Selection

Given the ability to realise physical waveforms with spectral notches as described in the previous section, we now turn to the problem of determining the notch dispositions (locations/widths). While the optimal solution is desired in theory, a ‘good enough’ solution is actually preferred to minimise the latency one can expect in a dynamic environment.

A multi-objective optimisation scheme was proposed in [30, 31] that seeks to balance the maximisation of SINR, in the form of acceptable interference in the band, against the maximisation of contiguous radar bandwidth. Furthermore, low-decision latency is achieved through a rapid band aggregation scheme analogous to the human thalamus [32] that performs data reduction prior to optimisation.

Here the FSS algorithm is used to identify the locations and widths of spectral regions that require notching in an efficient manner by reducing the number of frequency bins needed to analyse the spectrum. The reduction is a consequence of combining frequency bins having similar power levels, ultimately producing alternating groups of low- and high-power ‘meso-bands’ [31], where this term is used to indicate a collection of similar frequency bins (or ‘micro-bands’). These meso-bands are then combined as appropriate to determine the final sub-bands where notches are needed.

As a brief summary of [31], given an observed sampled spectrum $\Theta = \{\theta_1, \dots, \theta_N\}$ of size N (e.g. through a periodogram or by averaging multiple shorter periodograms), this approach first applies a threshold T_f in order to group the samples (micro-bands) into meso-bands of like samples. Specifically, a low-power meso-band (LPM) is defined as a contiguous set of frequency samples whose values are all below the threshold T_f while a high-power meso-band (HPM) is defined as a contiguous set of frequency samples whose values are all above the threshold T_f . In [31] the threshold was set based on an extensive set of training data for a large variety of scenarios. Here a simpler approach of X dB down from the maximum RFI was used, with $X = 15$ dB arbitrarily selected (see Fig. 1).

Each meso-band index $q \in [1, \dots, Q]$ is parameterised by start frequency index $S(q)$ and end frequency index $E(q)$. The number of frequency samples in the q th meso-band is

$L(q) = E(q) - S(q) + 1$, which defines the corresponding meso-band bandwidth as

$$B_q = L(q)\Delta f, \quad (8)$$

for Δf the frequency resolution.

The FSS algorithm then enforces a minimum allowable meso-band width of B_{\min} such that the radar spectrum is not overly fragmented (e.g. see [36]), which in this context of spectral notching provides adequate room for the tapered transition described in (4). This minimum bandwidth translates to the discrete frequency length

$$L_{\min} = \left\lceil \frac{B_{\min}}{\Delta f} \right\rceil, \quad (9)$$

where $\lceil \bullet \rceil$ is the ceiling operator. If an LPM has a discrete length $L(q) < L_{\min}$, then it is merged with adjacent HPMs until the minimum length is achieved. The resulting set of frequency samples parameterise the r^{th} sub-band Φ_r with the start and end frequency indices $S(r)$ and $E(r)$, where $r \in [1, \dots, R]$ and $R \leq Q$. Fig. 1 illustrates an example involving 5 sub-bands determined by FSS when two OFDM signals are present and B_{\min} is set to 4 MHz. See [30, 31] for a detailed description of this approach.

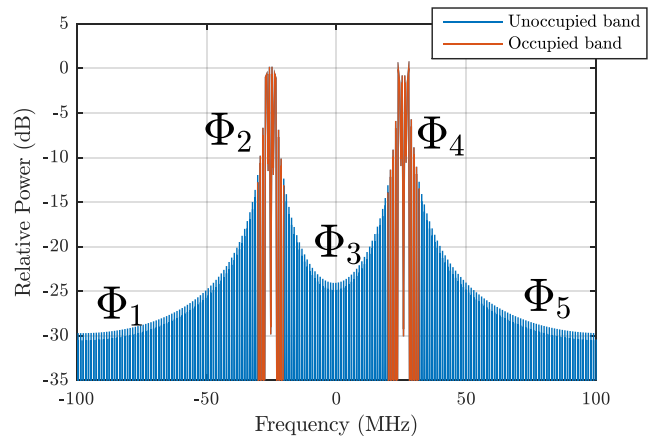


Fig. 1. FSS-determined sub-bands for two OFDM signals, where $\{\Phi_1, \Phi_3, \Phi_5\}$ represent unoccupied sub-bands and $\{\Phi_2, \Phi_4\}$ represent occupied sub-bands

4. Physical Realization of FM Noise Waveforms

The optimisation process outlined in Section 2 serves to produce constant modulus, pulse-agile FM noise waveforms that are well-contained spectrally, are amenable to high power amplification, and produce deep spectral notches. We now consider the behaviour of these waveforms when physically generated and captured using RF test equipment, which highlights some important factors to be considered when deploying such an approach.

4.1 Hardware Implementation

The optimised FM waveforms realized by (4), and with deeper spectral notches via (7), were physically generated using a Tektronix AWG70002A Arbitrary Waveform Generator (AWG) and captured (mean value) by a Rohde & Schwarz FSW Real-time Spectrum Analyser (RSA). A total of $M = 2500$ pulsed waveforms were digitally up-sampled to 10 GS/s, up-converted to a centre frequency of 3.55 GHz, and

then generated by the AWG. Each pulsed waveform has a duration of $T = 2 \mu\text{s}$ and a 3 dB bandwidth of $B = 100 \text{ MHz}$, yielding a time bandwidth product of $BT = 200$ per pulse and an overall dimensionality of $MBT = 5 \times 10^5$ for the entire CPI, thus realising a coherent integration gain of about 57 dB. The pulse repetition interval (PRI) is $40 \mu\text{s}$ so that the 2500 waveforms constitute a CPI of 100 ms. Receive capture (either free-space or in loopback configuration) is subsequently performed by the RSA through I/Q sampling at 2×10^8 sample/s. Note that the RSA has an analysis bandwidth limitation of 160 MHz that introduces increased spectral roll-off at the edges of the band (on receive only).

4.2 Digital Up-sampling and Up-conversion

Digital up-sampling and up-conversion is necessary for direct implementation of waveforms on the AWG. Here each of the waveforms produced by (7) is up-sampled digitally in Matlab™ from a sampling rate of $F_s = 2 \times 10^8$ sample/s to the up-sampled rate of $F_{us} = 10^{10}$ sample/s through spline interpolation of phase. Any subsequent amplitude variations are removed to re-enforce constant modulus. Since the discretised waveform at rate F_s is already over-sampled with respect to 3 dB bandwidth, the up-sampled waveform at F_{us} is clearly even more so, and consequently high fidelity is maintained in so far as spectral containment is concerned.

It has been observed, however, that spline phase interpolation tends to severely degrade notch depth in the up-sampled waveform, possibly due to the associated image rejection filtering. To mitigate this degradation, additional alternating projections similar to (1) and (2) are performed at the higher sampling rate. Denote $\tilde{\mathbf{x}}_{p=0,m}$ as the up-sampled version of version $\mathbf{x}_{L,m}$ from (7). The desired spectral notch depth is reacquired through P iterations of the alternating application of

$$\tilde{\mathbf{v}}_{p+1,m} = \mathbb{F}^{-1} \left\{ \tilde{\mathbf{g}} \odot \exp \left(j \angle \mathbb{F} \left\{ \tilde{\mathbf{x}}_{p,m} \right\} \right) \right\} \quad (10)$$

and

$$\tilde{\mathbf{x}}_{p+1,m} = \tilde{\mathbf{u}} \odot \exp \left(j \angle \tilde{\mathbf{v}}_{p+1,m} \right), \quad (11)$$

where $\tilde{\mathbf{g}}$ and $\tilde{\mathbf{u}}$ are discretised versions of $|G(f)|$ and $u(t)$, respectively, at the up-sampled rate. Note that the prior resolution from the alternating projection scheme in (1) and (2) does permit $\tilde{\mathbf{g}}$ to simply have 0's in the notch regions and 1's elsewhere without appreciably altering the spectrum shape aside from notch depth. In other words, the notch depth is reacquired without further shaping of the rest of the spectrum.

Fig. 2 illustrates the root mean square (RMS) spectra computed over $M = 2500$ unique waveforms at each stage of this optimisation, up-sampling, and re-notching process. For $BT = 200$, the procedure in (1)-(7) is applied to produce a single notch of width $B/10$ on the right-most edge of the 3 dB bandwidth at $+0.5B$. After $L = 100$ iterations of (7), an RMS notch depth of 50 dB relative to the peak is obtained for the original discretised waveforms (blue trace in Fig. 2). However, when these waveforms are up-sampled by a factor of 50 (red trace in Fig. 2) the resulting RMS notch depth is only about 20 dB relative to the peak. At the higher rate the 50 dB notch is obtained once again (yellow trace in Fig. 2) after performing $P=100$ iterations of (10) and (11). Finally, this re-notched up-sampled waveform is digitally up-

converted to realize a 3.55 GHz centre frequency when generated by the AWG.

The AWG generated waveform (yellow in Fig. 2) also shows quite good spectral containment. In terms of normalised frequency, a roll-off rate of about 60 dB per decade is observed beyond $\pm B$ (the original spectral limits at the lower sampling rate) until around $\pm 5B$ (not shown), at which point the roll-off rate gradually flattens out until settling to a relative power level of about -65 dB . In other words, the spectral containment of this waveform compares rather well to spectral mask requirements (e.g. [37]).

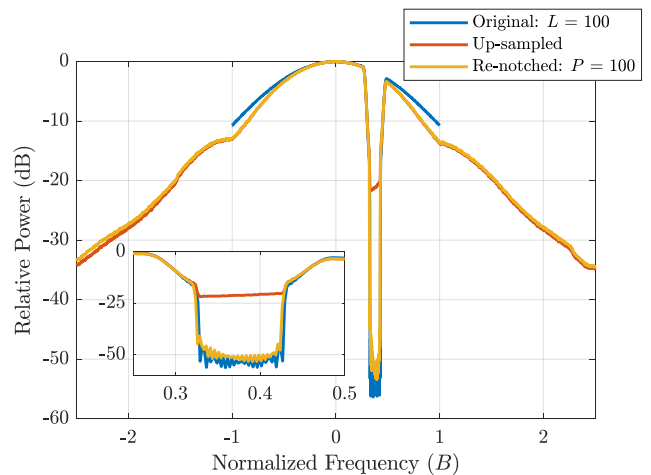


Fig. 2. RMS spectra of original discretised notched waveform (blue), the up-sampled waveform (red), and after re-notching the up-sampled waveform (yellow). The inset shows a detail view of the notch

The process described above, with the attendant higher computational cost to implement (10) and (11) at the higher sampling rate, is necessary because of the digital up-sampling and up-conversion required for a direct digital implementation on the AWG. In contrast, analogue up-conversion would eliminate the need for up-sampling, though distortion effects within the analogue transmit chain could still fill in the notch to some degree.

4.3 Practical Amplification Effects

While the initial optimisation process in (1) and (2) does produce a waveform amenable to the rigors of amplification by a power amplifier (PA) operating in saturation, it has been observed that the depth of spectral notches tend to be susceptible to PA distortion effects [23]. For example, using a Mini-Circuits ZHL-42W medium/high-PA in a loopback configuration, it was found that when operating beyond the 3 dB compression point of the PA the notch depth experienced $\sim 5 \text{ dB}$ of degradation relative to the case in which the PA was operated in the linear region. It is expected that the high-power PAs used in many deployed/legacy systems, many of them tube-based, would realise further degradation.

5. Assessment of Notched FM Noise Waveforms

Many design parameters can be varied when forming spectral notches in these optimised FM noise waveforms. The following discusses these different attributes and experimentally evaluates the individual impact of each on radar performance.

5.1 Tapering of Spectral Notches

It was shown in [23] that enforcement of a rectangular spectral notch such as implied by (3) produces a $\sin(x)/x$ roll-off in autocorrelation sidelobes. This result is not unexpected when one considers that the placement of a rectangular notch is akin to adding a signal that possesses a rectangular frequency response, albeit with the opposite sign. It was likewise demonstrated that tapering of the notch through (4) partially eliminates this sidelobe increase, as illustrated in Figs. 3 and 4 for loopback captured versions of the waveforms. Here the RMS power spectrum is depicted along with the associated aggregate autocorrelation response (i.e. their average) for a set of $M = 2500$ waveforms, with the notch tapers based on a Tukey window. It is observed that the tapered notch cases (yellow and purple) realize significantly lower sidelobes than the rectangular notch case (red), and even approach the performance of the case without a notch (blue). For the remainder of the attributes examined a $B/16$ Tukey taper is employed.

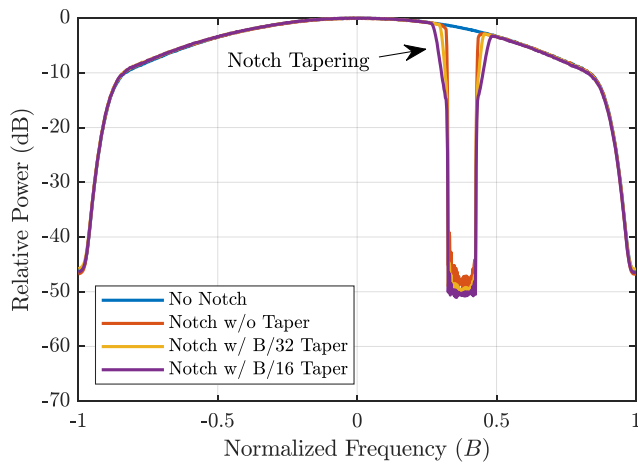


Fig. 3. RMS power (for 2500 unique waveforms) comparing spectral notch tapering to the rectangular notch and the absence of a notch. The sharp roll-off is due to the limited analysis bandwidth of the RSA used for loopback capture

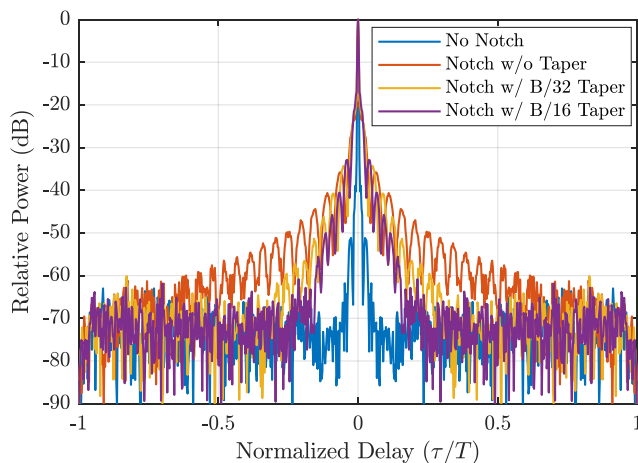


Fig. 4. Aggregate autocorrelation (for 2500 unique waveforms) comparing spectral notch tapering to the rectangular notch and the absence of a notch

5.2 Doppler Spreading Induced by Notch Hopping

It was also shown in [23] (for a continuous wave (CW) version of FM noise) that hopping the spectral notch within the CPI to address dynamically changing interference causes smearing of the delay-Doppler point spread function. Fig. 5 illustrates this effect for a loopback capture of pulsed waveforms when the notch location changes 10 times during the CPI. For a CPI of 100 ms, each notch persists in one of 10 spectral locations for 10 ms. The ten locations are chosen randomly, are allowed to overlap with one another, and each is only used once during the CPI. Standard matched filter pulse compression and Doppler processing is performed, with a Taylor window applied across the pulses to suppress Doppler sidelobes. Compared to the baseline case (not shown) of a static notch location that produces a thumbtack response, it is observed in Fig. 5 that a noticeable amount of smearing occurs when the notch moves during the CPI.

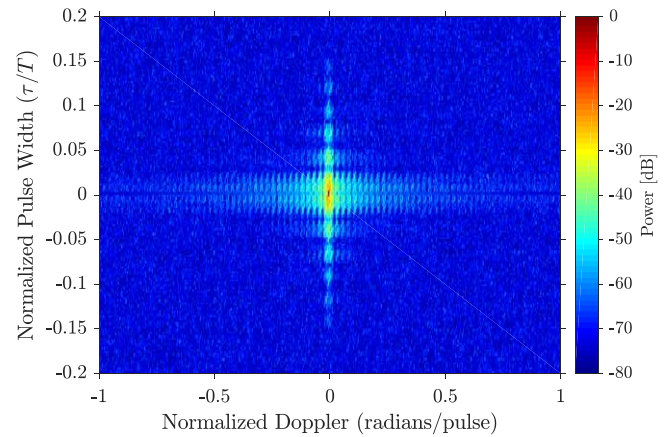


Fig. 5. Delay-Doppler point spread function when the spectral notch hops ten times during a 100 ms CPI

The smearing incurred by allowing the notch to move during the CPI is exacerbated if the rate of movement is increased. Fig. 6 shows the delay-Doppler point spread function when 100 different notch locations are chosen at random without repeat for the 100 ms CPI, such that each now persists for 1 ms. The matched filtering and Taylor-windowed Doppler processing are the same. The smearing is clearly more severe in this case, which suggests that there may be practical limits to how rapidly the notch could change. Techniques to compensate for this effect are a topic of ongoing investigation.

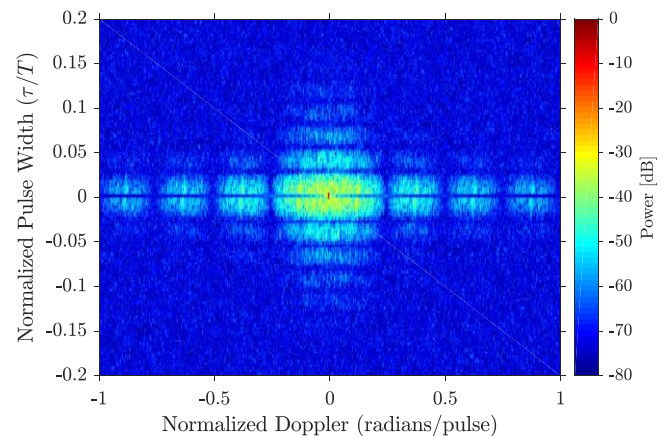


Fig. 6. Range-Doppler point spread function when the spectral notch hops 100 times during a 100 ms CPI

5.3 Impact of Notch Width Modulation

The notched waveform design formulation in Section 2 relies on the availability of knowledge regarding where spectral notches are required. For spectrum sensing and estimation approaches such as FSS described in Section 3 and [31], the act of estimating interference in real data introduces the possibility of estimation error even for stationary RFI. While the SINR degradation related either to underestimating interference (missed detection) or overestimating interference (false alarm) is relatively obvious, there also exists the prospect of correctly estimating RFI, but with varying bandwidth from pulse to pulse. This issue arises simply due to the fact that the spectral roll-off of real signals do not fit perfectly within discrete frequency bins, and the subsequent effect is a modulation of the notch width during the CPI.

To examine this effect, quasi-narrowband RFI taking the form of eight OFDM subcarriers, spaced 1 MHz apart, was generated and inserted within the 3 dB bandwidth of the radar. The FSS algorithm was again used to identify the notch region on an individual pulse basis. While the OFDM subcarriers did remain stationary during the CPI, natural variations in the spectral roll-off caused the estimated width to change. As a control case, a second set of PRO-FM waveforms was generated with the notch width held constant during the CPI.

These two sets of notched PRO-FM radar emissions were implemented on the AWG, captured in loopback on the RSA, and then matched filtered and summed to produce the zero-Doppler delay response (i.e. the aggregate autocorrelation). Fig. 7 depicts the result for these two cases for CPIs of $M = 2500$ unique pulsed waveforms.

It is interesting to note that the modulated notch width, which can be expected to occur in practice, is actually marginally superior to the control case in which no notch width modulation occurs. The observed reason for this outcome is that the random perturbation of the notch edge serves to further smooth out the tapered transition region around the notch. It has also been noted that Doppler smearing resulting from this effect is essentially negligible.

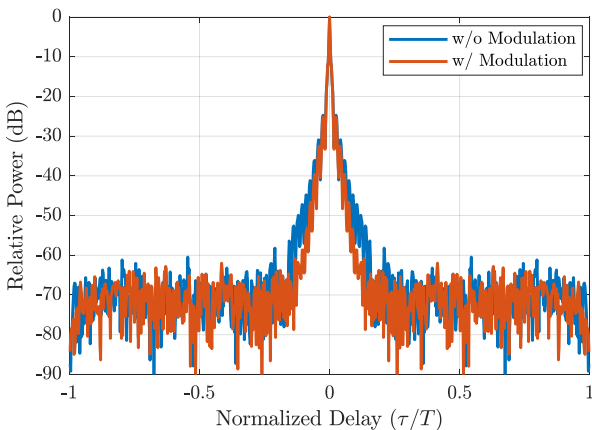


Fig. 7. Aggregate autocorrelation response (for 2500 unique waveforms) comparing a modulated notch width to a constant notch width

5.4 Notching in Static vs. Agile Waveforms

Finally, it is instructive to ascertain how the spectral notching of these agile FM noise waveforms compares to traditional schemes involving notching of a single waveform

that is repeated over the CPI. To do so, a notch width of $B/10$ and Tukey taper of $B/16$ width are incorporated into $M = 2500$ unique PRO-FM waveforms, with the notch located inside the 3 dB passband. The same notch (except for the spectral taper) is also incorporated into a standard linear frequency modulation (LFM) waveform having the same BT , and this waveform is repeated for the same size CPI.

Fig. 8 illustrates the aggregate autocorrelation response after matched filtering the M pulses and summing (so zero-Doppler) for these two kinds of notched waveforms. An unmodified LFM response is included for reference. It is observed that notching the LFM waveform realises significantly higher sidelobes relative to the unmodified LFM case. This result agrees with those found using a similar approach in [12, 15]. However, not only are the notched FM noise waveforms more robust than notched LFM, on an overall CPI basis they are even better than the original LFM waveform when no notching was employed. Simply put, the randomisation of sidelobes due to the changing waveform structure provides a sidelobe decoherence benefit when the matched filter responses are combined in Doppler processing.

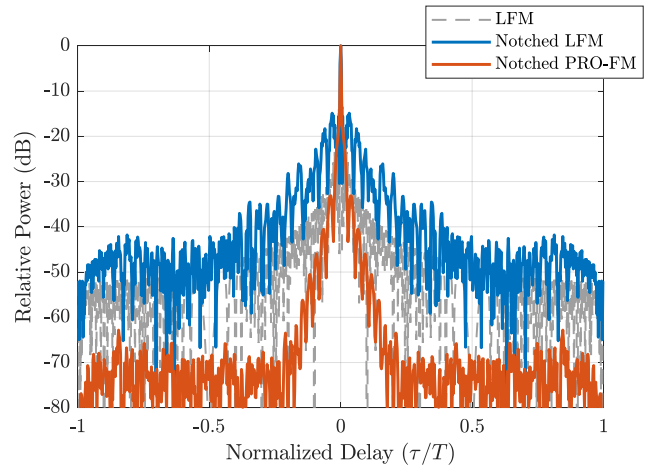


Fig. 8. Comparison between notched LFM, notched PRO-FM, and unmodified LFM in terms of simulated aggregate autocorrelation response (for 2500 unique waveforms)

6. Assessing Notch Interference Rejection

The main application for the placement of spectral notches in radar waveforms is the avoidance of in-band RFI. It was shown in [25] that a notch coinciding with the spectral location of high-power narrowband RFI provides a direct benefit to target detection via reduction of interference in the matched filter response.

Here OFDM interference comprised of eight subcarriers with 1 MHz spacing was generated on the AWG and captured in loopback on the RSA. PRO-FM waveforms with and without a notch at the same spectral location were similarly generated and captured in loopback. These two sets of waveforms were synthetically combined with the interference at signal-to-interference (SIR) levels of 0 dB, -20 dB, and -40 dB (determined according to per-sample average power).

Fig. 9 shows the aggregate autocorrelation response for all six cases (two waveform sets for each of three SIR levels). It is clearly evident that spectral notching (dashed traces) provides a significant advantage over the notch-free cases (solid traces) when the interference is high (-20 dB (red) and

-40 dB (yellow) SIR). When the interference and signal powers are commensurate (0 dB, blue) the slower sidelobe roll-off due to notching realizes a higher response near the mainlobe, though further out in range the benefit of notching is still observed.

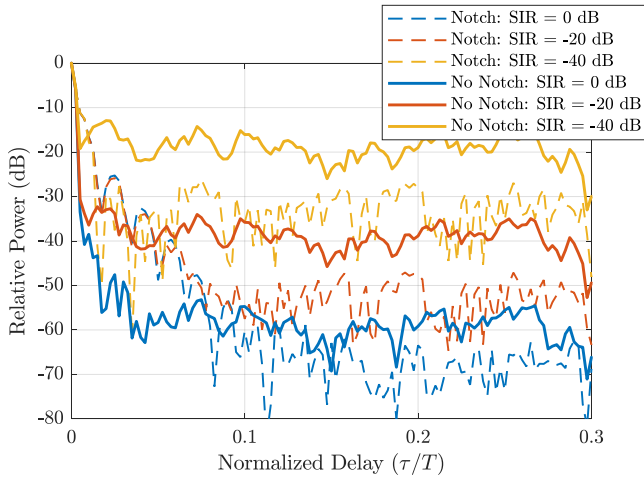


Fig. 9. Aggregate autocorrelation response (for 2500 unique waveforms) comparing notched and un-notched responses in the presence of RFI for three different SIR values

7. Cognitive notching for MTI

Now consider how this form of cognitive spectral notching performs for a MTI application. The RFI in this context is once again an OFDM signal that is cohabitating the 3 dB bandwidth B occupied by the radar. In [26] the impact of a single interference band was investigated. Here the OFDM signal resides in two disjoint bands, each consisting of four adjacent subcarriers that comprise separate contiguous bandwidths of 4 MHz. Each subcarrier is modulated by random symbols from a 4-QAM (quadrature amplitude modulated) constellation at a symbol rate of 1 MHz.

The transmitter (AWG) and receiver (RSA), configured as shown in Fig. 10, were situated on the roof of Nichols Hall on the University of Kansas campus, thus emulating a radar on a stationary platform. The field of view includes the intersection of 23rd and Iowa Streets in Lawrence, KS, which experiences a decent amount of automobile traffic that is close to being radially oriented to the transmitter/receiver site.

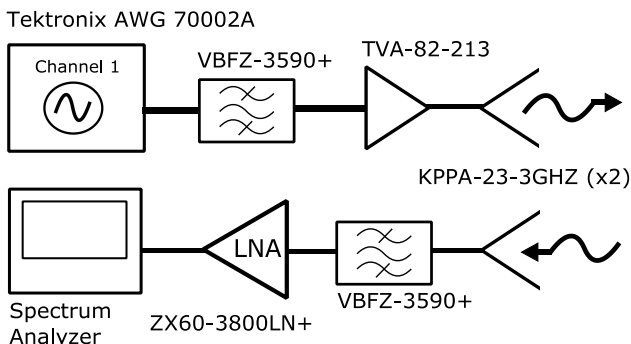


Fig. 10. Open-air hardware setup

To fully characterize the interaction of this form of cognitive radar with the in-band interference, different interference arrangements are generated and the FSS

algorithm is applied on a per-pulse basis to identify the occupied RFI bands. Each pulsed radar waveform is then designed to notch the portion(s) of spectrum determined by FSS. These waveforms are transmitted as described above to collect free-space measurements of moving vehicles. The loopback measurements of interference and the free-space radar measurements are then combined synthetically in MatlabTM to determine how well notching mitigates the interference. The radar measurements are also evaluated individually (without interference included) to assess the trade-off notching imposes.

Three interference scenarios are examined. In Case 1 the two RFI bands are located symmetrically about the centre frequency and are stationary in frequency over the entire CPI. In Case 2 the RFI bands frequency hop to random, distinct locations and the radar waveform adapts its notch locations instantaneously (assumes spectrum sensing and notching can occur without latency). In Case 3 the RFI bands frequency hop to random, distinct locations and the update of the notch location has a latency of one PRI. For all cases, the FSS algorithm is used to identify the HPMs of the spectrum using a power threshold T_f set to be 15 dB below the average peak power of the OFDM subcarriers. The minimum allowable sub-band size B_{\min} is set to 4 MHz.

Fig. 11 shows the measured OFDM spectrum from Case 1 along with the full-band and notched PRO-FM spectra for a single PRI captured in loopback. The sharp roll-off of the measured spectrum is caused by the limited analysis bandwidth (160 MHz) of the RSA. The FSS algorithm identifies the portions of the OFDM spectra that are above the threshold and establishes the notch widths accordingly. Note that these OFDM signals are not that well-contained spectrally, which means that leakage interference still occurs despite the notching. If the interference possessed better spectral containment this leakage degradation would largely be avoided.

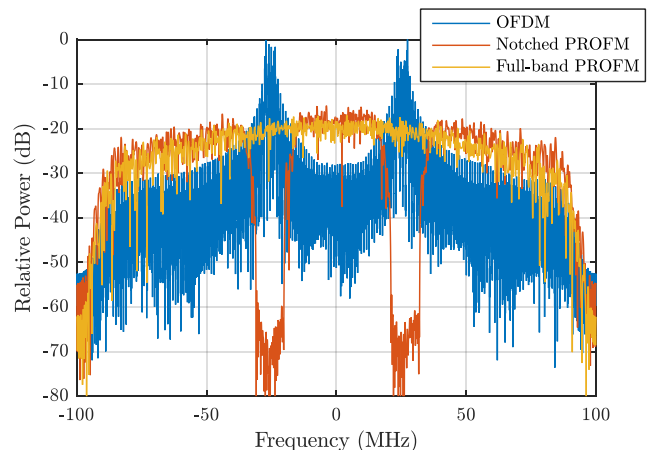


Fig. 11. Power-normalised measured spectra of the OFDM interference, notched PRO-FM (adapted using FSS), and full-band PRO-FM for 1 PRI of Case 1

The experimental timing diagram for Case 2 is illustrated in Fig. 12, where the two OFDM signals move after every fourth PRI. To facilitate comparison between the full-band and notched PRO-FM waveforms for the same illuminated scene, the two are interleaved. Note that in instances in which the RFI bands hop near one another (e.g. RFI Hop 2 in Fig.

12) FSS may combine the identified meso-bands into a single sub-band for notching.

A total of 5000 interleaved pulses were transmitted for each case, with 2500 each for full-band and notched PRO-FM. Accounting for the interleaving, the PRI is defined as the time period between each pair of pulses and is set to 40 μ s. Each pulse has a duration of 2 μ s and a 3 dB bandwidth of 100 MHz. Consequently, both sets of radar waveforms have $BT = 200$. The CPI for each set of waveforms was 100 ms. The OFDM signals and radar emissions were generated at a centre frequency of 3.55 GHz and the resulting I/Q data were captured at a sample rate of 200 MHz for both loopback and free-space measurements.

On receive, matched filtering was performed using loopback captured versions of the emitted waveforms to account for hardware imperfections. Since there was no platform motion, clutter cancellation was performed by a simple projection of the zero-Doppler response along with a Taylor window to suppress Doppler sidelobes.

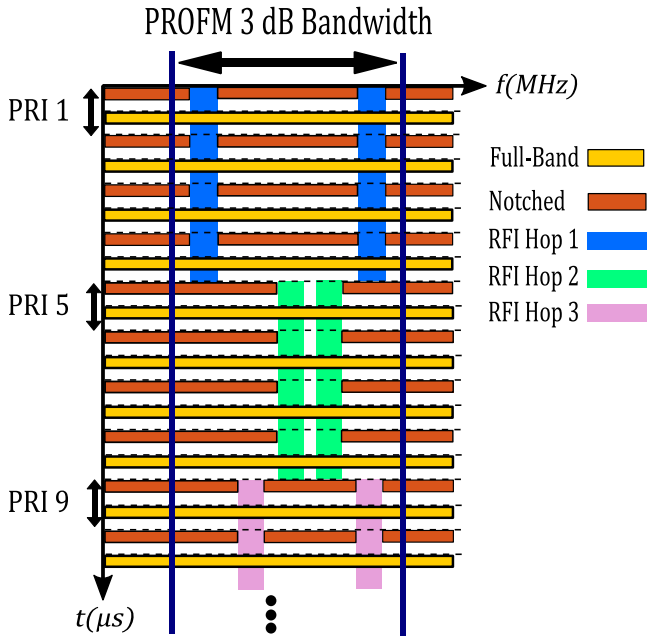


Fig. 12. Timing diagram for Case 2 in which the radar adapts new notches instantly when the interference location changes (no latency). The full-band and notched PRO-FM pulses are interleaved to illuminate the same scene

A. Stationary Interference

Fig. 13 shows the measured range-Doppler response after clutter cancellation for the full-band PRO-FM waveform when no RFI is included. Multiple vehicles are clearly visible here as moving targets. It is useful to compare this result with the notched PRO-FM response in Fig. 14 that likewise does not include RFI. Note that a slight spreading in range, due to higher near-in sidelobes and not degraded resolution, is observed in the latter due to notching, which agrees with the results in [25].

The loopback-measured stationary RFI (Case 1) was power scaled and then synthetically combined with the free-space measurements. It is assumed that the measured clutter power is sufficiently greater than the noise power for the latter to be neglected. Thus the ‘received’ SIR is defined here as the RMS power of the received radar backscatter signal

(excluding direct path) divided by the RMS power of the OFDM interference.

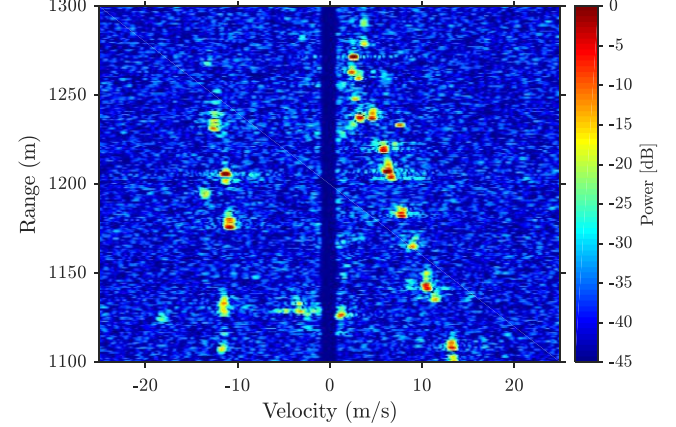


Fig. 13. Range-Doppler plot of full-band PRO-FM with no injected RFI (Case 1)

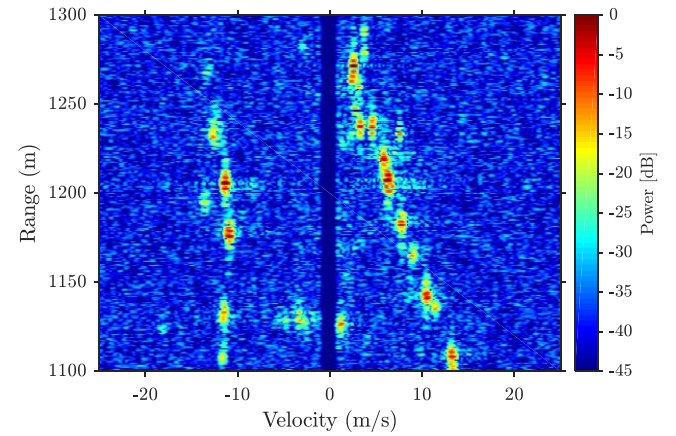


Fig. 14. Range-Doppler plot of notched PRO-FM with no injected RFI for Case 1 (obtained using stationary RFI)

Figs. 15 and 16 show the measured range-Doppler plots for the full-band and notched PRO-FM waveforms when RFI is injected that is 20 dB greater than the radar receive echoes (i.e. a received signal-to-interference ratio of $SIR_{rec} = -20$ dB). By inspection, the notched waveforms experience some degradation by way of an increased background response due to interference leakage. In contrast, the full-band waveforms are greatly affected by the interference, so much so that the moving targets are essentially obscured beyond recognition.

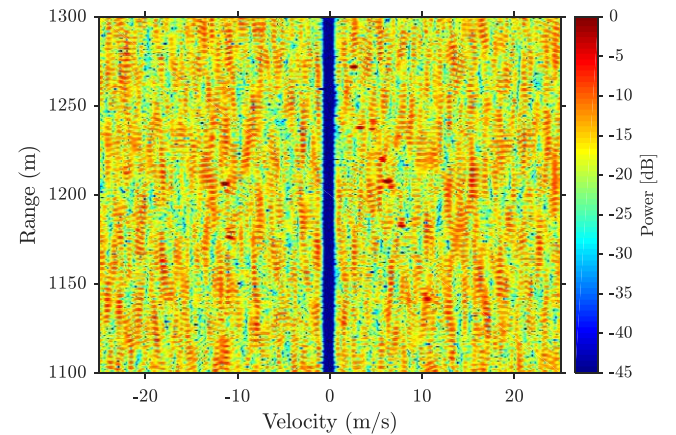


Fig. 15. Range-Doppler plot of full-band PRO-FM with injected stationary RFI at $SIR = -20$ dB (Case 1)

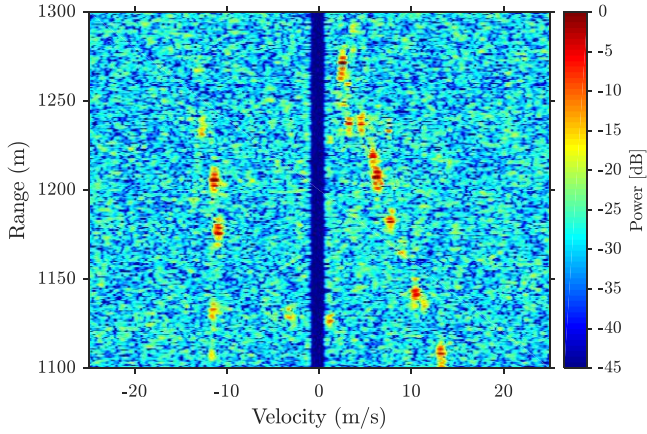


Fig. 16. Range-Doppler plot of notched PRO-FM with injected stationary RFI at SIR = -20 dB (Case 1)

A useful metric to assess the impact of interference that is facilitated by this synthetic combination, along with the individual impact of hopping notches, is

$$\Delta = \frac{I_{\text{meas}}}{I_{\text{baseline}}}, \quad (12)$$

where I_{meas} is the average power measured for each scenario in the range/Doppler regions that do not contain discernible targets or the clutter notch. The value I_{baseline} is then the particular value of I_{meas} for the full-band, no RFI scenario (e.g. Fig. 13). Consequently, the metric in (12) represents the change in the background response induced by RFI or spectral notches (or combination thereof) that would subsequently impact downstream CFAR (constant false alarm rate) detection.

Table I shows that, compared to the full-band scenario, the stationary notch of Case 1 incurs a little more than 1 dB of degradation in terms of an increased noise floor when no RFI is present. However, when RFI is present the full-band waveforms realize a 23 dB sensitivity penalty while the notched waveforms only suffer nearly 11 dB, a net difference of 12 dB. The notched waveform clearly provides a benefit, even when the RFI has poor spectral containment.

Table I. Impact of interference and notching for Case 1

	I_{meas}	Δ
Full-band, no RFI (baseline)	-39.5 dB	--
Notched, no RFI	-38.2 dB	+1.3 dB
Full-band, with RFI	-16.5 dB	+23.0 dB
Notched, with RFI	-28.6 dB	+10.9 dB

B. Hopping Interference, Instantaneous Response

Now consider the scenario in which the interference and associated waveform notches frequency hop at a rate of once every four PRIs, with the radar (hypothetically) able to respond instantaneously to the new notch locations (Case 2). The interference hopping and full-band/notched waveform interleaving conform to the timing arrangement in Fig. 12. The RFI-free versions of the full-band and notched waveform MTI responses are shown in Figs. 17 and 18, respectively. In particular, it is noted that moving the notch location during the CPI (Fig. 18) produces a Doppler smearing effect that is completely independent of RFI (since none is present at the moment). Compensating for this smearing is a topic of ongoing investigation.

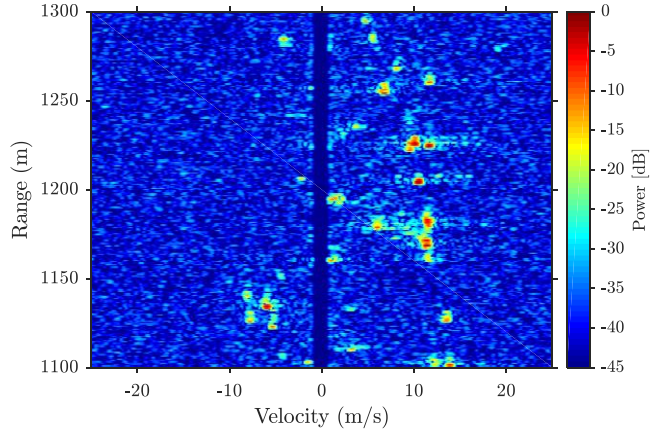


Fig. 17. Range-Doppler plot of full-band PRO-FM with no injected RFI (Case 2)

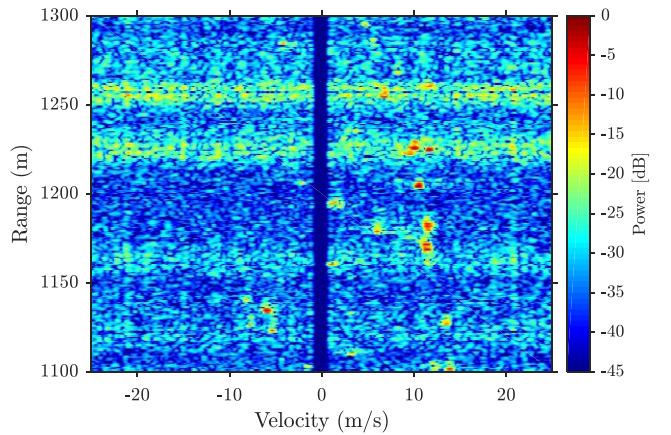


Fig. 18. Range-Doppler plot of frequency hopping notched PRO-FM with no injected RFI (Case 2)

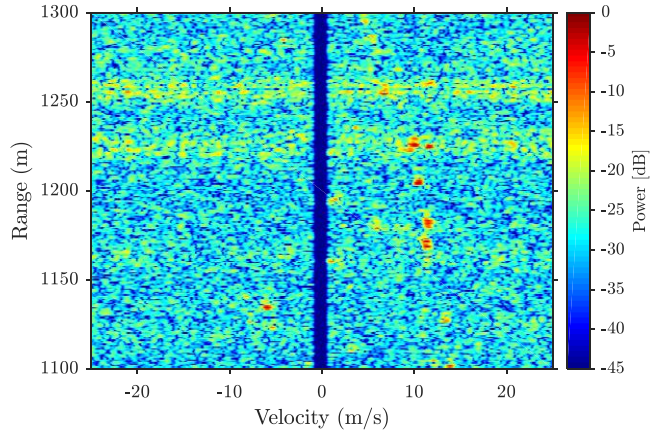


Fig. 19. Range-Doppler plot of frequency hopping notched PRO-FM with injected RFI at SIR = -20 dB (Case 2)

In Table II, it is interesting to observe that the hopping notch (without RFI) yields a nearly 8 dB increase in the noise floor, which is actually uncanceled clutter that is smeared across the range and Doppler. When frequency hopping RFI is present, again with $\text{SIR}_{\text{rec}} = -20$ dB, the full-band response (not shown) experiences the same 23 dB degradation as before (like Fig. 15). In contrast, Fig. 19 illustrates the MTI performance of the notched waveforms, which now realises $\Delta = 12$ dB, only 1 dB worse than the stationary RFI case.

Also, while it is a bit difficult to visualise due to the differences between the illuminated scenes and the presence of Doppler smearing in this case, the moving targets in Fig. 18 do not experience the higher near-in range sidelobes that were evident in Fig. 14. This result occurs because the notch hopping better mitigates the coherence of the associated sidelobes.

Table II. Impact of interference and notching for Case 2

	I_{meas}	Δ
Full-band, no RFI (baseline)	-39.7 dB	--
Notched, no RFI	-31.8 dB	+7.9 dB
Full-band, with RFI	-16.6 dB	+23.1 dB
Notched, with RFI	-27.7 dB	+12.0 dB

C. Hopping Interference, Delayed Response

Finally, where the previous case assumed the radar possesses clairvoyant knowledge of the interference spectral locations, now consider the impact of latency in the spectrum sensing/waveform design process. For the sake of illustration it is assumed that the radar requires one PRI before it can respond to a change in the interference location(s), with Fig. 20 depicting the timing diagram for this scenario.

Note that between one RFI hop and the next, if an RFI band randomly moves into a spectral location in proximity to an immediately previous location, then the RFI may still be suppressed despite the latency (as shown between RFI Hop 2 and Hop 3 in Fig. 20). This coincidental notching is a random, improbable occurrence that will not affect a significant number of pulses in the CPI.

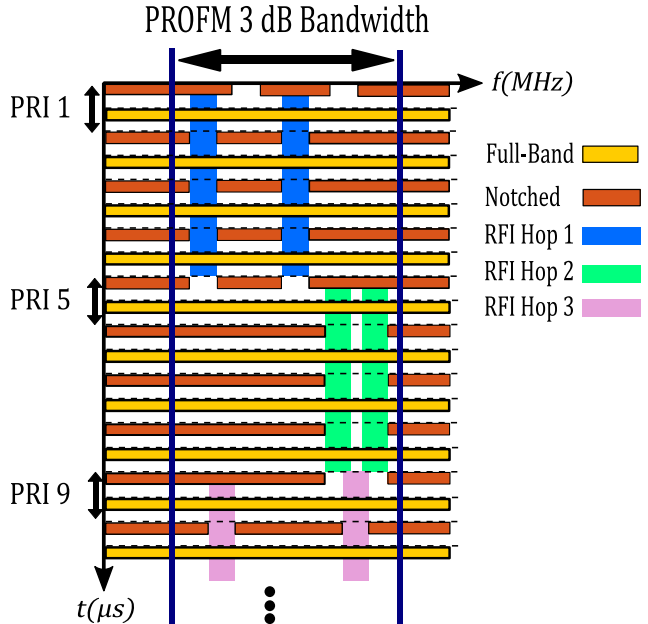


Fig. 20. Timing diagram for Case 3 (notch locations experience a one PRI delay when the interference changes)

Figures 21 and 22 illustrate the full-band and notched responses when RFI is not present. In Table III, the hopped notching again incurs just a little under 8 dB of degradation due to clutter smearing. When RFI is present, the full-band result (not shown) again experiences the same 23 dB loss in sensitivity.

Table III. Impact of interference and notching for Case 3

	I_{meas}	Δ
Full-band, no RFI (baseline)	-39.7 dB	--
Notched, no RFI	-32.3 dB	+7.3 dB
Full-band, with RFI	-16.6 dB	+23.1 dB
Notched, with RFI	-21.9 dB	+17.8 dB
Notched, with RFI, blanked	-29.4 dB	+10.3 dB

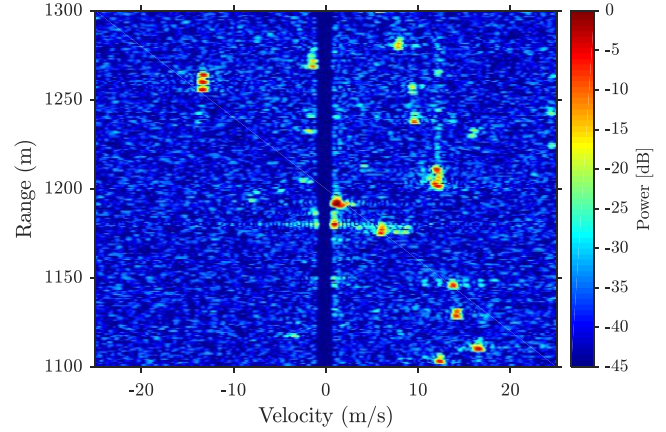


Fig. 21. Range-Doppler plot of full-band PRO-FM with no injected RFI for (Case 3)

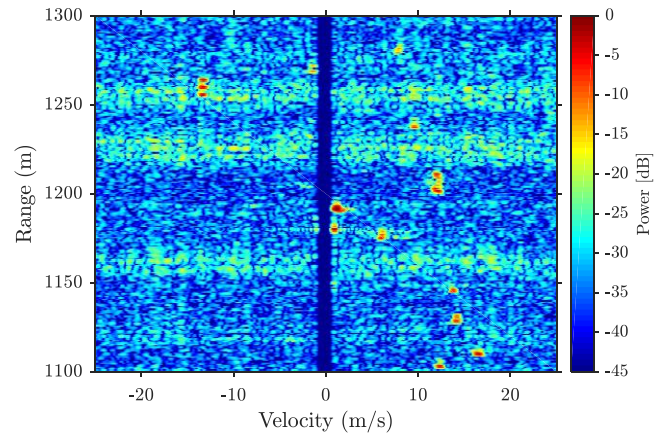


Fig. 22. Range-Doppler plot of frequency hopping notched PRO-FM with no injected RFI and one PRI delay (Case 3)

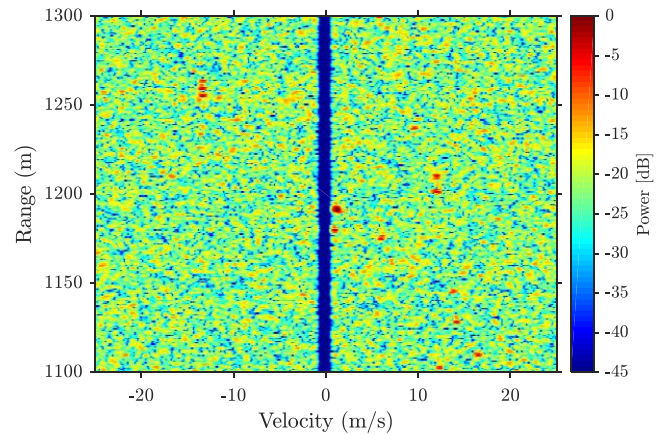


Fig. 23. Range-Doppler plot of frequency hopping notched PRO-FM with injected RFI at $SIR = -20$ dB and one PRI delay (Case 3)

Fig. 23 shows the notched response for a one PRI delay when interference is injected. Due to the response latency of

the cognitive system, Δ has increased from 12 dB in Case 2 to almost 18 dB. This result emphasises the importance of quickly adapting the waveform to changing RFI.

One possible way in which unavoidable latency may be addressed is to employ a ‘pulse blanking’ procedure similar to that performed for sidelobe blanking [33]. Given knowledge of how quickly the cognitive system can respond to changing RFI (here one PRI was considered), that number of pulsed echoes can simply be excluded from Doppler processing after each RFI change. Doing so would trade a loss in coherent signal integration in return for avoiding the spike in interference for those pulses due to notch/interference mismatch.

In the example depicted above, blanking 1 PRI out of every 4 pulses results in an expected signal power loss of $10\log_{10}(3/4) \approx 1.25$ dB. However, as Fig. 24 shows (compared to Fig. 23) the associated reduction in processed RFI is well worth this trade. In fact, the resulting residual RFI that is measured by Δ is now commensurate with the previous cases (it is actually the lowest of the three cases, though this distinction is not statistically significant)

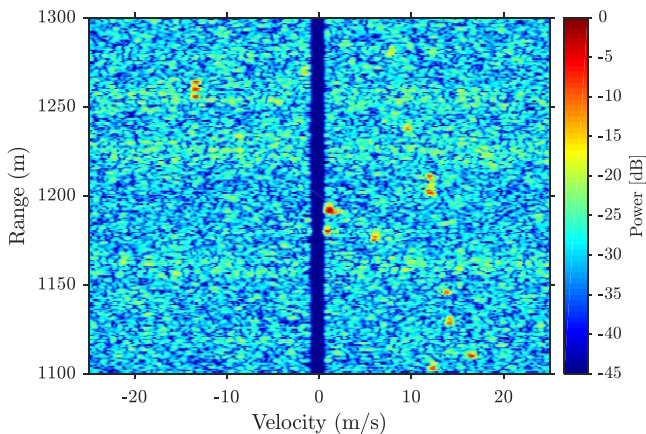


Fig. 24. Range-Doppler plot of frequency hopping notched PRO-FM with injected RFI of SIR = -20 dB, one PRI delay, and blanking the echoes of every fourth pulse

8. Conclusions

It has been experimentally demonstrated that incorporating hopped spectral notches into a non-repeating FM noise radar emission based on FSS facilitates the proactive suppression of dynamic narrowband RFI for the MTI application. Many practical factors contribute to the efficacy of this approach, including the shape of the notch, maintaining notch depth when generating the final emitted waveform, transmitter distortion, Doppler smearing due to notch hopping to address changing RFI, and notch width modulation.

It was illustrated how the notching of FM noise waveforms largely avoids the limitations that have previously been observed when notching static, repeated waveforms in a CPI. It was likewise shown how the matched filter response of notched waveforms provides significant RFI suppression in comparison to full-band waveforms.

Finally, loopback-captured RFI combined with free-space experimental measurements based on correspondingly notched waveforms has demonstrated the benefit of cognitive spectral notching for real-time, proactive RFI mitigation. These results verified the Doppler smearing effect when

notches are forced to move in order to address changing RFI. It was likewise shown that latency in the spectrum sensing/waveform design process incurs a significant interference penalty, though this degradation can be offset by using a simple blanking procedure.

9. Acknowledgments

This work was supported by the U.S. Army Research Office under Grant # W911NF-15-2-0063.

10. References

- [1] S. Haykin, “Cognitive radar: a way of the future,” *IEEE Signal Processing Mag.*, vol. 23, no. 1, pp. 30-40, Jan. 2006.
- [2] J. Guerci, *Cognitive Radar: The Knowledge-Aided Fully Adaptive Approach*, Artech House, Norwood, MA, USA, 2010.
- [3] S. Haykin, *Cognitive Dynamic Systems: Perception-Action Cycle, Radar, and Radio*, Cambridge University Press, Cambridge, UK, 2012.
- [4] A.F. Martone, “Cognitive radar demystified,” *URSI Radio Science Bulletin*, no. 350, pp. 10-22, Sept. 2014.
- [5] K.L. Bell, C.J. Baker, G.E. Smith, et al., “Cognitive radar framework for target detection and tracking,” *IEEE J. Selected Topics Signal Processing*, vol. 9, no. 8, pp. 1427-1439, Dec. 2015.
- [6] P. Stinco, M.S. Greco, F. Gini, “Spectrum sensing and sharing for cognitive radars,” *IET Radar, Sonar & Navigation*, vol. 10, no. 3, pp. 595-602, Feb. 2016.
- [7] B.H. Kirk, K.A. Gallagher, J.W. Owen, et al., “Cognitive software defined radar for time-varying RFI avoidance,” *IEEE Radar Conf.*, Oklahoma City, OK, USA, Apr. 2018.
- [8] H. Griffiths, L. Cohen, S. Watts, et al., “Radar spectrum engineering and management: technical and regulatory issues,” *Proc. IEEE*, vol. 103, no. 1, pp. 85-102, Jan. 2015.
- [9] M. Labib, V. Marojevic, A.F. Martone, et al., “Coexistence between communications and radar systems – a survey,” *URSI Radio Science Bulletin*, vol. 2017, no. 362, pp. 74-82, Sept. 2017.
- [10] S.D. Blunt, E.S. Perrins, eds., *Radar & Communication Spectrum Sharing*, IET, 2018.
- [11] M.J. Lindenfeld, “Sparse frequency transmit-and-receive waveform design,” *IEEE Trans. Aerospace & Electronic Systems*, vol. 40, no. 3, pp. 851-861, July 2004.
- [12] I. W. Selesnick, S. U. Pillai and R. Zheng, “An iterative algorithm for the construction of notched chirp signals,” *IEEE Intl. Radar Conf.*, Washington, DC, USA, May 2010.
- [13] M.R. Cook, T. Higgins, A.K. Shackelford, “Thinned spectrum radar waveforms,” *Intl. Waveform Diversity & Design Conf.*, Niagara Falls, ON, Canada, Aug. 2010.

- [14] K. Gerlach, M.R. Frey, M.J. Steiner, et al., "Spectral nulling on transmit via nonlinear FM radar waveforms," *IEEE Trans. Aerospace & Electronic Systems*, vol. 47, no. 2, pp. 1507-1515, Apr. 2011.
- [15] I.W. Selesnick and S.U. Pillai, "Chirp-like transmit waveforms with multiple frequency-notches," *IEEE Radar Conf.*, Kansas City, MO, USA, May 2011.
- [16] S.W. Frost and B. Rigling, "Sidelobe predictions for spectrally-disjoint radar waveforms," *IEEE Radar Conf.*, Atlanta, GA, May 2012.
- [17] C. Nunn, L.R. Moyer, "Spectrally-compliant waveforms for wideband radar," *IEEE Aerospace & Electronic Systems Mag.*, vol. 27, no. 8, pp. 11-15, August 2012.
- [18] L.K. Patton, B.D. Rigling, "Phase retrieval for radar waveform optimization," *IEEE Trans. Aerospace & Electronic Systems*, vol. 48, no. 4, pp. 3287-3302, October 2012.
- [19] L.K. Patton, C.A. Bryant, B. Himed, "Radar-centric design of waveforms with disjoint spectral support," *IEEE Radar Conf.*, Atlanta, GA, USA, May 2012.
- [20] T. Higgins, T. Webster, A.K. Shackelford, "Mitigating interference via spatial and spectral nulling," *IET Radar, Sonar & Navigation*, vol.8, no.2, pp.84-93, Feb. 2014.
- [21] A. Aubry, A. De Maio, Y. Huang, et al., "A new radar waveform design algorithm with improved feasibility for spectral coexistence," *IEEE Trans. Aerospace & Electronic Systems*, vol. 51, no. 2, pp. 1029-1038, Apr. 2015.
- [22] J. Jakobosky, S.D. Blunt, A. Martone, "Incorporating hopped spectral gaps into nonrecurrent nonlinear FMCW radar emissions," *IEEE Intl. Workshop Computational Advances in Multi-Sensor Adaptive Processing*, Cancun, Mexico, Dec. 2015.
- [23] J. Jakobosky, B. Ravenscroft, S.D. Blunt, et al., "Gapped spectrum shaping for tandem-hopped radar/communications & cognitive sensing," *IEEE Radar Conf.*, Philadelphia, PA, May 2016.
- [24] A. Aubry, A. De Maio, A. Farina, "Optimization theory-based radar waveform design for spectrally dense environments," *IEEE Aerospace & Electronic Systems Mag.*, vol. 31, no. 12, pp. 14-25, Dec. 2016.
- [25] B. Ravenscroft, S.D. Blunt, C. Allen, et al., "Analysis of spectral notching in FM noise radar using measured interference," *IET Intl. Conf. Radar Systems*, Belfast, UK, Oct. 2017.
- [26] J.W. Owen, B. Ravenscroft, B.H. Kirk, et al., "Experimental demonstration of cognitive spectrum sensing & notching for radar," *IEEE Radar Conf.*, Oklahoma City, OK, USA, Apr. 2018.
- [27] J. Jakobosky, S.D. Blunt, B. Himed, "Waveform design and receive processing for nonrecurrent nonlinear FMCW radar," *IEEE Intl. Radar Conf.*, Washington, DC, May 2015.
- [28] J. Jakobosky, S.D. Blunt, B. Himed, "Spectral-shape optimized FM noise radar for pulse agility," *IEEE Radar Conf.*, Philadelphia, PA, May 2016.
- [29] C.A. Mohr, P.M. McCormick, S.D. Blunt, "Optimized complementary waveform subsets within an FM noise radar CPI," *IEEE Radar Conf.*, Oklahoma City, OK, USA, Apr. 2018.
- [30] A. Martone, K. Ranney, "Fast technique for wideband spectrum sensing," *IEEE Antennas & Propagation Intl. Symp.*, Memphis, TN, USA, July 2014.
- [31] A. Martone, K. Ranney, K. Sherbondy, et al., "Spectrum allocation for non-cooperative radar coexistence," *IEEE Trans. Aerospace & Electronic Systems*, vol. 54, no. 1, pp. 90-105, Feb. 2018.
- [32] W.M. Connelly, M. Laing, A.C. Errington, et al., "The thalamus as a low pass filter: filtering at the cellular level does not equate with filtering at the network level," *Frontiers in Neural Circuits*, vol. 9, no. 89, pp. 1-10, Jan. 2016.
- [33] W.L. Melvin, J.A. Scheer, eds., *Principles of Modern Radar, vol. II: Advanced Techniques*, SciTech Publishing, 2013, Chap. 12.
- [34] A. Johnston, "Improvements to a pulse compression radar matched filter," *Radio and Electronic Engineer*, vol. 53, no. 4, pp. 138-140, Apr. 1983.
- [35] S.D. Blunt, M. Cook, J. Jakobosky, et al., "Polyphase-coded FM (PCFM) radar waveforms, part I: implementation," *IEEE Trans. Aerospace & Electronic Systems*, vol. 50, no. 3, pp. 2218-2229, July 2014.
- [36] P.S. Tan, J.M. Stiles, S.D. Blunt, "Physically realizing an optimized sparse spectrum via joint design of a collection of FM waveforms," *IEEE Radar Conf.*, Oklahoma City, OK, Apr. 2018.
- [37] 'Manual of Regulations and Procedures for Federal Radio Frequency Management', https://www.ntia.doc.gov/files/ntia/publications/redbook/2015-09/5_15_9.pdf, accessed 08 February 2018.